3D Problems of Rotating Detonation Wave in a Ramjet Engine Modeled on a Supercomputer

Valeriy F. Nikitin[1,2], *Yurii G. Filippov*[1], *Lyuben I. Stamov*[1,2], *Elena V. Mikhalchenko*[1,2]

A rotating detonation engine (RDE) combustion chamber was modeled in the work numerically using 3D geometry. The RDE is a new type of engines capable to create higher thrust than the traditional ones, which are based on the combustible mixture deflagration process. In the numerical experiment, different scenarios of the engine performance were obtained. The calculations were made at a compact supercomputer APK-5 with a peak performance of 5.5 Tera Flops.

Keywords: Mathematical Modeling, Detonation, Deflagration, RDE, Ramjet.

Introduction

The optimization of modern engines based on the traditional design is now close to its technological limit. The engines performance may be increased only with the use of radically new technical solutions [1]. One of those solutions is the development of detonation engines; we deal with an engine with a rotating detonation [2]. The rotating detonation engine is being investigated extensively during the last decades; see works [3, 4].

The numerical modeling of the processes in a combustion chamber is an important stage in the investigation of its design and further usage. The mathematical model includes equations for multicomponent gas mixture, it considers chemical reactions and turbulent transport of mass, momentum and energy. In order to resolve such events as detonation cells development and thin wave con-figurations, one should have a rather thin computational mesh, and it contributes to the complexity. Therefore, the problem should be solved using big computational resources, high precision approximation schemes, and effective parallelization methods: OpenMP, MPI, CUDA, etc. In order to solve such problems, the authors have created a parallel code with the AUSM [5], the MUSCL [6] methods incorporated. The current research uses the OpenMP version of the computer program.

1. Mathematical Model

The mathematical model contains the governing equations (differential and algebraic), boundary and initial conditions. The details of the numerical realization together with the computational mesh design and the placement of variables on the mesh, is a subject of the numerical model.

1.1. The Balance Equations

To model a multicomponent gas mixture, we use the following system of balance equations:

$$\frac{\partial \rho_k}{\partial t} + \frac{\partial}{\partial x_j}\left(\rho_k u_j\right) - \frac{\partial J_{kj}}{\partial x_j} = \dot{\omega}_k, \tag{1}$$

---

[1]Lomonosov Moscow State University, Moscow, Russia
[2]SRISA RAS, Moscow, Russia

$$\frac{\partial \rho u_i}{\partial t} + \frac{\partial}{\partial x_j}\left(\rho u_i u_j\right) + \frac{\partial p}{\partial x_i} - \frac{\partial \tau_{ij}}{\partial x_j} = 0, \tag{2}$$

$$\frac{\partial E_T}{\partial t} + \frac{\partial}{\partial x_j}\left((E_T + p)u_j\right) - \frac{\partial}{\partial x_j}\left(J_{Tj} + u_i \tau_{ij}\right) = \dot{Q}. \tag{3}$$

Here ρ_k is partial density of a species k, J_{kj} are vector components of the species k diffusion flux, $\dot{\omega}_k$ is the intensity of the species k origination in chemical reactions, ρ is the gas mixture density, u_j are vector components of gas velocity, p is the mixture pressure, τ_{ij} are the tensor components of viscous and turbulent stresses, E_T is total energy of the gas volume unit consisting of thermal, chemical, kinetic and turbulent energy, J_{Tj} are vector components of the energy diffusion flux, $\dot{Q}$ is the heat flux from an external source.

1.2. Additional Algebraic Relations

Density of mixture is a sum of partial densities, and it is useful to introduce two types of concentrations: mass shares of species, and molar densities:

$$\rho = \sum_{k=1}^{N_C} \rho_k, \quad Y_k = \frac{\rho_k}{\rho}, \quad X_k = \frac{\rho_k}{W_k}. \tag{4}$$

Here: Y_k is the mass share of the species k, X_k is the molar density (in terms of many works on chemical kinetics it is named a molar concentration), W_k is the molar mass of a species.

The pressure p is defined as the spherical part of the stresses tensor, with the opposite sign. It is a sum of thermal pressure $\hat{p}$ of perfect gases mixture, and an additive corresponding to turbulent pulsations, which is modeled by means of the turbulent energy per mass unit K:

$$p = \hat{p} + \frac{2}{3}\rho K, \quad \hat{p} = R_G T \sum_{k=1|}^{N_C} X_k. \tag{5}$$

The total energy of a volume unit is the following sum:

$$E_T = E + \rho \frac{u^2}{2} + \rho K, \quad u^2 = u_j u_j. \tag{6}$$

The total energy E_T is therefore the sum of internal (thermal and chemical) energy, kinetic, and turbulent energy. The internal energy of a volume unit is modeled as follows:

$$E = \sum_{k=1}^{N_C} X_k E_k = \sum_{k=1}^{N_C} X_k \left(\hat{H}_k(T) - 1\right). \tag{7}$$

Here, E_k is an internal energy of a species mole, $\hat{H}_k$ is dimensionless enthalpy of a species containing the formation enthalpy at a reference temperature T_{ref} (chemical energy). Those functions are the basis of the species thermodynamic description; for many species, they are either tabulated, or approximated with polynomials. In the current research, they are taken from [7]; their format (two temperature interval) is described in [8] and [9]. We joined those temperature intervals into a single, and obtained the polynomial coefficients using the linear regression analysis based on the least squares technique.

1.3. Chemical Kinetics

In the current research, the chemical sources $\dot{\omega}_k$ depend on temperature T and the set of molar densities X_k; the sum of those sources is zero due to the law of mass conservation in chemical reactions:

$$\dot{\omega}_k = W_k \hat{\omega}_k(T, X_j), \quad \sum_{k=1}^{N_C} \dot{\omega}_k = 0. \tag{8}$$

Here $\hat{\omega}_k$ is the intensity of a species mole origination in a volume unit.

Some more strict laws for chemical interactions exist, e.g. the conservation of mass for each element. Those laws are considered in the chemical mechanism, and sometimes can reduce the computation effort and increase the precisity. A general form for the chemical sources is usually complex, and it consists of many nonlinear terms; a typical expression is as follows:

$$\hat{\omega}_k = \sum_{r=1}^{N_R} \nu_{rk} \omega_r, \quad \omega_r = M_r(X_j) \left[k_{Fr}(M_r, T) \prod_{i=1}^{N_C} X_i^{\alpha_{ri}} - k_{Br}(M_r, T) \prod_{i=1}^{N_C} X_i^{\beta_{ri}} \right]. \tag{9}$$

Here, ω_r is the reaction r speed (intensity), ν_{rk} is an algebraic stoichiometric coefficient for a species k in the reaction r, this coefficient is positive for the species being produced, and negative for those being consumed. M_r is the influence coefficient of non-changing components, which is equal to unity in the lack of such an influence, k_{Fr} is the direct reaction speed coefficient; it usually depend on temperature only, but for some falloff reactions it depends on M_r, k_{Br} is the reverse reaction speed, α_{rk} are degrees for species in a direct reaction (usually but not always they are non-zero for the input species), β_{rk} are the degrees for the reverse reactions.

In case of elementary reactions, the degrees for species in the expression (9) are the same with the input and output stoichiometric coefficients. The reverse reaction speed coefficients were calculated to provide the reach of the dynamical chemical equilibrium in the case of zero external fluxes and constant density and internal energy; the following expression was used:

$$k_{Br} = k_{Fr} \exp \left[\sum_{k=1}^{N_C} \nu_{rk} \left(\dot{H}_k(T) - \dot{S}_k(T) - 1 \right) \right] \left(\frac{R_G T}{p_{ref}} \right)^{\nu_r}, \quad \nu_r = \sum_{k=1}^{N_C} \nu_{rk}. \tag{10}$$

The entropy dimensionless coefficients $\hat{S}_k$ are constructed like $\hat{H}_k$ from data in [7] using formulae from [9].

For each direct reaction, its coefficient is modeled with an extended Arrhenius formula:

$$k_{Fr} = A_r T^{B_r} \exp \left(-\frac{\Theta_r}{T} \right), \tag{11}$$

where the reaction activation temperature Θ_r is derived from the activation energy as $\Theta_r = E_{ar}/R_G$.

1.4. Turbulence Model and Transport

The current research uses the Wilcox ka-omega model [10]:

$$\frac{\partial \rho K}{\partial t} + \frac{\partial}{\partial x_j} (\rho K u_j) - \frac{\partial}{\partial x_j} \left((\mu + \sigma^* \mu_T) \frac{\partial K}{\partial x_j} \right) = \tau_{ij}^T \frac{\partial u_i}{\partial x_j} - \beta^* \rho K \omega, \tag{12}$$

$$\frac{\partial \rho \omega}{\partial t} + \frac{\partial}{\partial x_j} (\rho \omega u_j) - \frac{\partial}{\partial x_j} \left((\mu + \sigma \mu_T) \frac{\partial \omega}{\partial x_j} \right) = \alpha \frac{\omega}{K} \tau_{ij}^T \frac{\partial u_i}{\partial x_j} - \beta \rho \omega^2, \tag{13}$$

$$\mu_T = \rho \frac{K}{\omega}. \tag{14}$$

Here K is the kinetic energy of pulsations per mass unit, μ is the molecular viscosity of the gas mixture, μ_T is the turbulent (eddy) viscosity, τ_{ij}^T is the turbulent part of the stresses tensor, ω is the intensity of the turbulent energy decay (dissipation) far away from walls and in lack of the turbulent energy input sources, parameters

$$\alpha = \frac{5}{9}, \quad \sigma = \sigma^* = \frac{1}{2}, \quad \beta = \frac{3}{40}, \quad \beta^* = \frac{9}{100}$$

are constant parameters of the standard Wilcox model.

The turbulent part of the stresses tensor deviator is:

$$\tau_{ij}^T = \mu_T \left(\frac{\partial u_i}{\partial x_j} + \frac{\partial u_j}{\partial x_i} - \frac{2}{3} \frac{\partial u_k}{\partial x_k} \delta_{ij} \right) - \frac{2}{3} \rho K \delta_{ij}, \tag{15}$$

where δ_{ij} is the Kronecker symbol.

The molecular viscosity of the gas mixture is calculated using the pure species viscosity $\mu_k(T)$ and molar densities X_k as:

$$\mu = \sum_{k=1}^{N_C} \frac{\mu_k X_k}{\displaystyle\sum_{j=1}^{N_C} \phi_{kj} X_j}. \tag{16}$$

The effective mixture viscosity is lower than the weighted average due to the binary influence coefficients ϕ_{kj}. A simple method to compute them was published in [11]:

$$\phi_{kj} = \frac{1}{\sqrt{8}} \left(1 + \frac{W_k}{W_j} \right)^{-\frac{1}{2}} \left[1 + \left(\frac{\mu_k}{\mu_j} \right)^{\frac{1}{2}} \left(\frac{W_j}{W_k} \right)^{\frac{1}{4}} \right]^2. \tag{17}$$

A molecular viscosity is calculated using physical molecular constants taken from the database [12], and the method of computation was taken from [11].

To calculate the fluxes of mass and energy J_{kj} and J_{Tj}, and the stresses tensor deviator τ_{ij}, we used a model taking into account the turbulent transport calculated by means of the Wilcox model [10]. In most cases, the turbulent transport supersedes the molecular, and the last is made using simplified technique using constant Prandtl Pr and Schmidt Sc numbers hypothesis [13]:

$$J_{kj} = \left(\frac{\mu}{\mathrm{Sc}} + \frac{\mu_T}{\mathrm{Sc}_T} \right) \frac{\partial Y_k}{\partial X_j}, \tag{18}$$

$$J_{Tj} = \left(\frac{\mu}{\mathrm{Pr}} + \frac{\mu_T}{\mathrm{Pr}_T} \right) \frac{\partial h}{\partial X_j} + (\mu + \mu_T) \frac{\partial K}{\partial x_j}, \tag{19}$$

$$\tau_{ij} = (\mu + \mu_T) \left(\frac{\partial u_i}{\partial x_j} + \frac{\partial u_j}{\partial x_i} - \frac{2}{3} \frac{\partial u_k}{\partial x_k} \delta_{ij} \right) - \frac{2}{3} \rho K \delta_{ij}. \tag{20}$$

Here, Sc_T, Pr_T are constant turbulent Schmidt and Prandtl numbers, h is the enthalpy per mass unit; the last is computed as follows:

$$h = \frac{R_G T}{\rho} \sum_{k=1}^{N_C} X_k \hat{H}_k(T). \tag{21}$$

1.5. The Species List and the Kinetic Mechanism

Hydrogen, oxygen and nitrogen were the initial and the inflow mixture components. In the process of combustion, besides the main product, water vapor, numerous products (radicals) are originated; at high temperature they still persist in the mixture, and at lower temperature they decay. We used the following set of species:

$$\{H_2O, OH, H, O, HO_2, H_2O_2; H_2, O_2, N_2\}.$$

The research used a kinetic mechanism described in the Maas & Pope work [14] (1992). The mechanism consisted of 20 reversible elementary reactions.

2. Results

A model combustion chamber of a ramjet detonation engine was treated as a test. Geometrically, it is a hollow cylinder with the cylindrical internal body, which ends up as a cone. The fuel flow into the chamber through numerous injectors (premixed rich composition $[H_2] : [O_2] = 3 : 1$, stagnant pressure 10 bar, stagnant temperature 258 K, Mach number at each orifice 1). At the initial instance, the chamber is filled with air at 1 bar pressure and 300 K temperature. The ignition is made by means of an external energy source into a small spherical portion: $r_{ign} = 2.5$ mm after a delay of 10 μs from the initial instance, and during $t_{ign} = 1$ μs, and with power per volume as high as $Q = 20$ kW/mm^3.
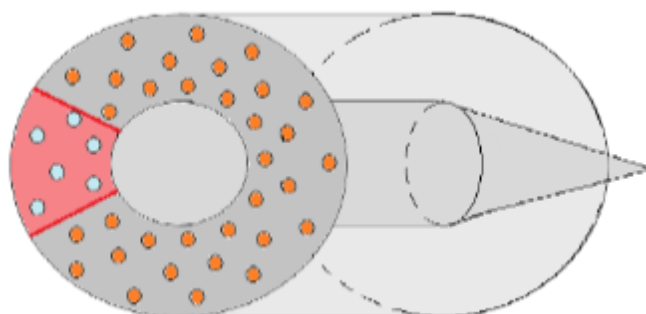

Figure 1. The combustion chamber geometry

The work area length was $L = 10$ cm, the maximal radius of the work area $R = 2.5$ cm, the inner body radius $R_b = 1.5$ cm, the inner body length without the terminating cone was $L_b = 3$ cm, the terminating cone length $L = 3$ cm, the number of injectors $N_r = 72$, their orifices radii were $r = 0.2$ cm. The test problem was solved on a structured cubic cells mesh made of $\approx 1.3 \cdot 10^6$ cells; the size of a cell was 0.5 mm.

In order to force detonation wave propagation in one direction, initially all the orifices were closed, then they are open in turn depending on their angular co-ordinate so that the whole ring is open by 30 μs from the beginning.

The Fig. 2 shows pressure in the ramjet engine combustion chamber for different times shown in a cross section OYZ at the distance of 0.5 cm from the injectors end.

One can see from the Fig. 2 that the detonation wave is formed after the ignition at 10 μs propagating in one direction (counter-clockwise) due to specific filling of the combustible mixture via the orifices (Fig. 2a). During the first circulation, its strength increases due to the increasing amount of fresh mixture ahead of it (Fig. 2b – Fig. 2c). After the detonation wave rotates once,
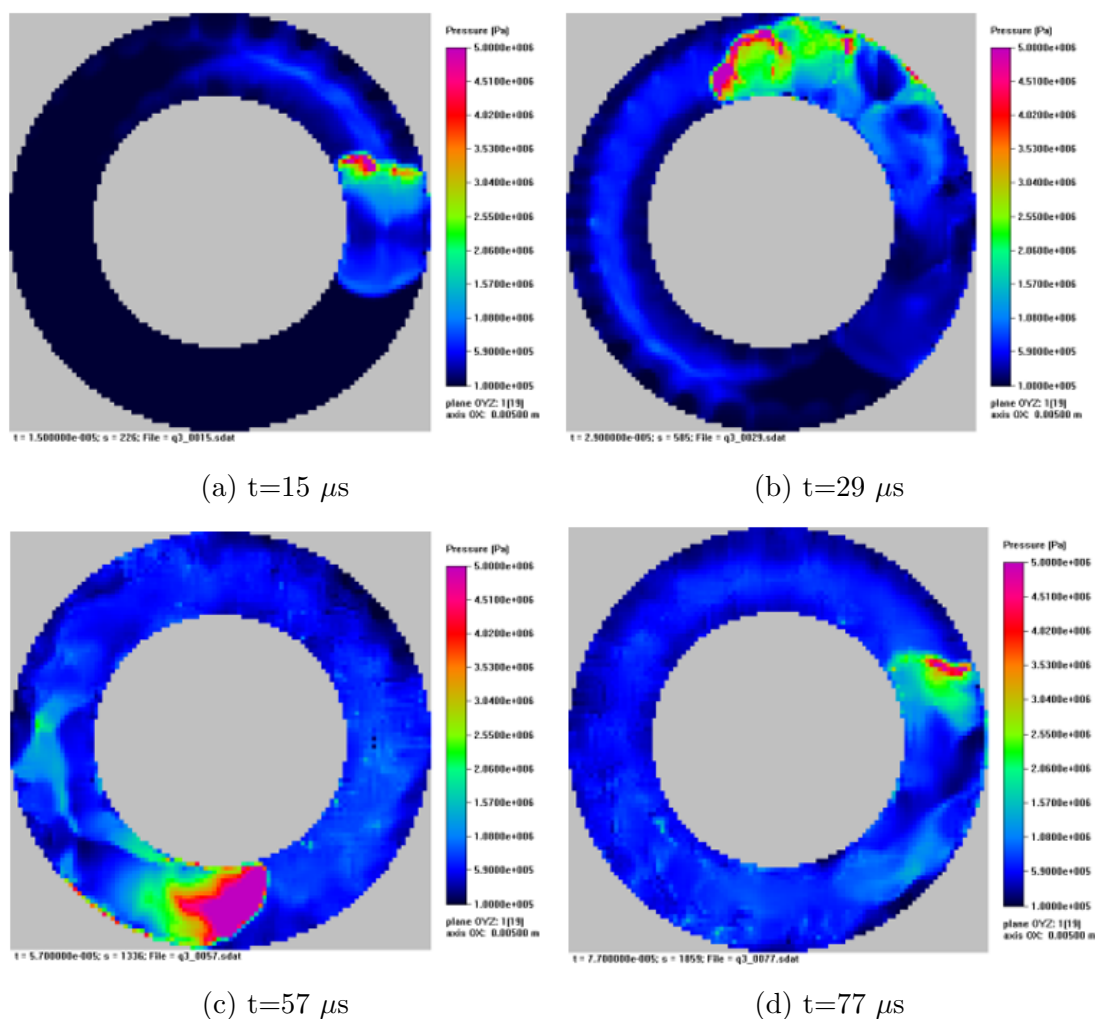
(a) t=15 μs

(b) t=29 μs

(c) t=57 μs

(d) t=77 μs

Figure 2. Pressure in the cross section

it goes weaker due to lower amount of combustible mixture ahead (Fig. 2d). Still it propagates without extinguishing.

The Fig. 3 shows temperature in this cross section at the same times.

The Fig. 3 shows that a portion of high temperature propagates counter-clockwise as the detonation wave, but the high temperature goes also clock-wise with lower velocity (Fig. 3a – Fig. 3b). Then, the temperature far behind the detonation wave decreases gradually due to the displacement of hot products of combustion with a fresh combustible mixture. This process is highly turbulent, and portions of hot products of combustion still remain in this cross section (Fig. 3c). When the detonation wave rotates once, the structure of the temperature field behind the wave in this cross section becomes more regular, but there still exist hot spots ahead of the wave; however, it propagates stably in the fresh mixture (Fig. 3d).

The Fig. 4 shows 3D distribution of pressure (Fig. 4a) and temperature (Fig. 4b), at $t = 57\,\mu$s from the beginning of the process.

One can see the spiral-shaped pressure profile (Fig. 4a); the lower portion of it in the vicinity of the orifices is a detonation wave, higher, it transfers to a shock wave. Other shock waves of smaller amplitude could be seen, generated by the initial gas mixture inflow. The temperature field (Fig. 4b) also demonstrates this spiral; one can see that the portion of fresh (cold) mixture ahead of the detonation wave is rather thin; the hot products of combustion originated at the
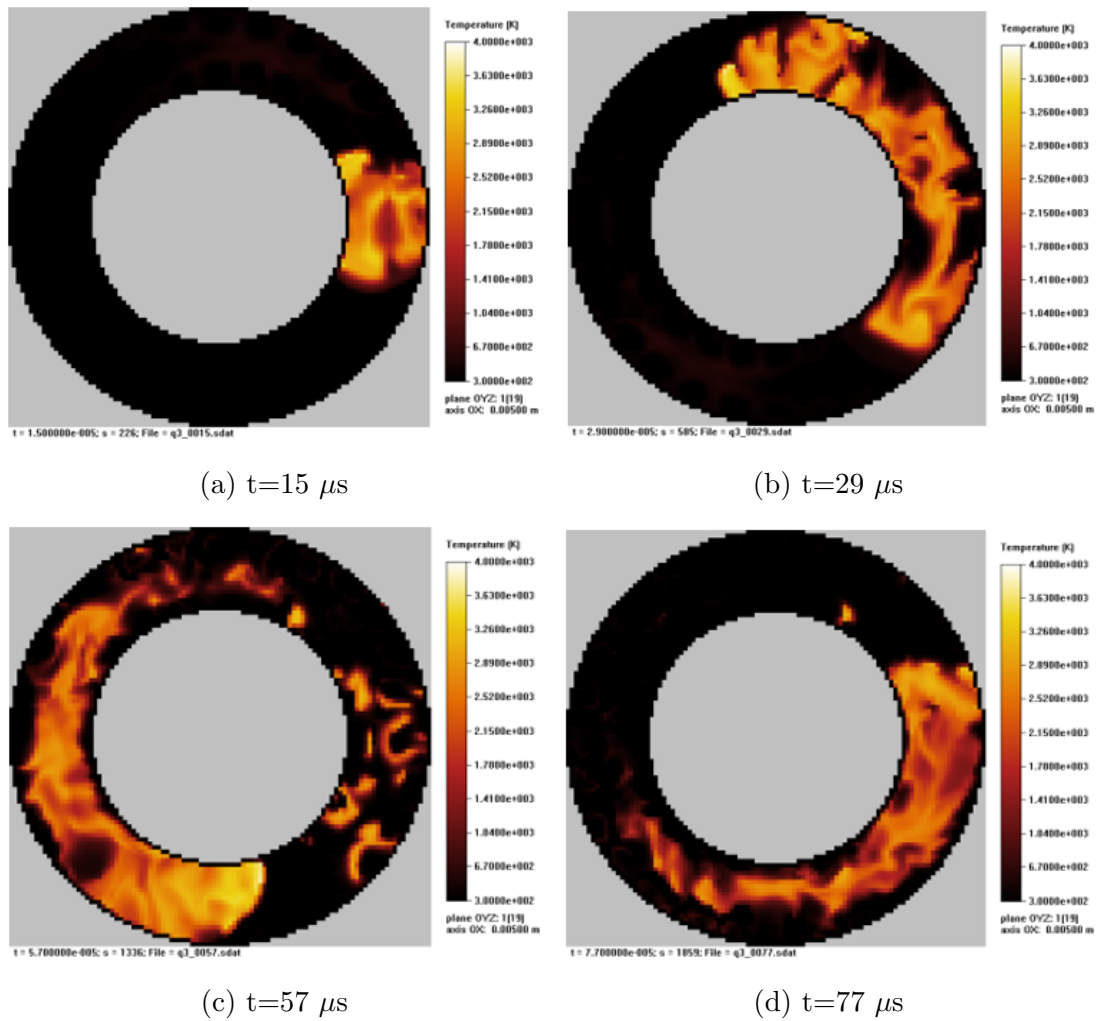
(a) t=15 μs

(b) t=29 μs

(c) t=57 μs

(d) t=77 μs

Figure 3. Temperature in the cross section

(a) 3D view of pressure at $t = 57$ μs

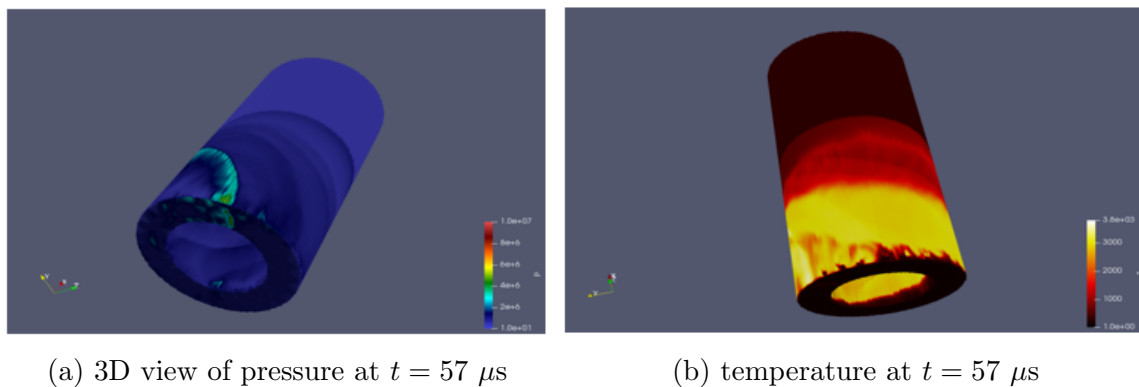(b) temperature at $t = 57$ μs

Figure 4. 3D view of pressure and temperature at $t = 57$ μs

first circulation of the detonation wave are depicted in yellow there, and they occupy the lower 1/3 of the combustion chamber by this time; the gas portion depicted in red is air heated by the primary shock generated by the inflow of combustible gases. The upper 1/3 of the combustion chamber is filled with cold undisturbed air: the shock wave has not reached it by $t = 57$ μs from the beginning of the process.

For the given parameter set, we obtained a detonation wave rotating around the bottom of the combustion chamber. In the beginning, a stable detonation wave originates, at first circulation its strength increases due to the increasing amount of fresh micture ahead of it. Then, it decreases due to much lower fresh mixture because the previous mixture was consumed one circulation before, and the new portion of it is much fewer than the initial. In some time after 70 μs the primary detonation wavet splits into two, even 3 waves, which then join into a single detonation wave. After that, in some time the process repeats: lateral waves reflections from walls contribute to it. As the result, we have obtained a galloping regime of rotating detonation.

2.1. The Calculating System

The calculations were performed at a computational system with two INTEL Xeon E5-2650 processors with 8 computational cores and 16 threads in each, and on a computational node of a native supercomputer APK-5 [15]. The fig. 5 shows the results of a computational test on both: acceleration due to the number of OpenMP threads, against a single thread. The time stepping algorithm was organized into 4 main cycles by cells and faces; the last cycle assembling all the fluxes together and creating the new state of parameters. The promotion to the 2nd order approximation in time was made repeating this algorithm once more with some modifications; the details are shown in [16] and [17].

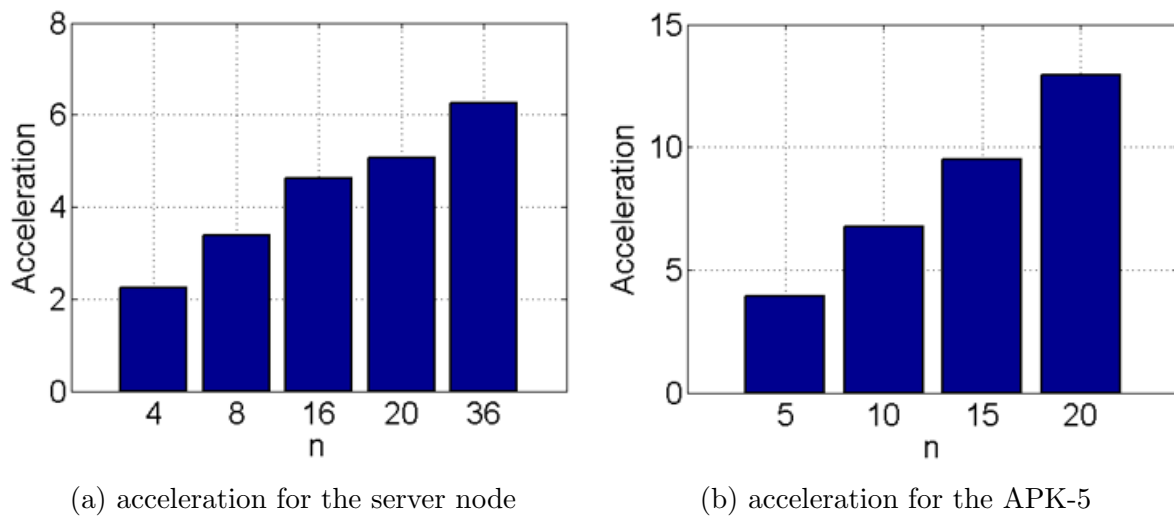The modeled configuration included more than 9 million cells.

(a) acceleration for the server node   (b) acceleration for the APK-5

Figure 5. Acceleration for the server node and for the APK-5

It is seen that for the number of processes given, the acceleration is near linear. This is due to the explicit numerical scheme used in calculations. We obtained more than 6 times acceleration on the server system, and more than 12 times acceleration on the computer APK-5. The APK-5 node acceleration is better due to high frequency of processors and its new architecture in comparison with the processors of the another server node.

In order to calculate the bigger devices, and/or to use better mesh refinement to resolve more details of the process, one should use all the computational nodes. To do this, it is worth to add the MPI parallelization paradigm into the computational algorithm.

Conclusions

The problem is computationally complex; the mathematical model includes multi-component gas dynamics, with the addition of the transport terms, the chemical kinetics, and the turbulence modeling. The following is obtained:

- The combustion chamber is a hollow cylinder; the inner body is cylindric, transfering to a cone. In case the fresh combustible mixture is inflown via the orifices which are open in turn, and not simultaneously, we obtained a detonation wave propagating in one direction.

- The detonation wave between two coaxial cylinders rotates consuming the fresh mixture. After one circulation, the thickness of the fresh mixture is rather small, due to a high velocity of detonation, and a small enough radius of circulation so that the time of one rotation was about 50 μs.

- Due to this, the strength of the detonation wave decreases after the first rotation. However, a stable inflow of cold fresh mixture causes the detonation wave to propagate even after the initial combustible mixture is consumed.

- Some hot spots initiate detonation in the fresh mixture ahead of the main wave so that it can split in two and even more other waves. The galloping detonation originated in some time.

- The numerical scheme was explicit, and the computational acceleration using OpenMP parallelization paradigm was nearly linear on both devices we have tested.

Acknowledgements

References

1. Bulat, P. V., Volkov, K. N.: Detonation jet engine. Part 2 construction features. International Journal of Environmental and Science Education (IJESE) 11(12), 5009–5019 (2016), https://istina.msu.ru/publications/article/42853937, accessed: 2018-05-15

2. Roy, G., Frolov, S.: Deflagrative and Detonative Combustion. Torus Press, Moscow (2010)

3. Wolanski, P., Kindracki, J., Fujiwara, T., Oka, Y., Shimauchi K.: An experimental study of rotating detonation engine. 20th International Colloquium on the Dynamics of Explosions and Reactive Systems 31 July – 5 August, 2005, Montreal, Canada (2005), http://www.icders.org/ICDERS2005, accessed: 2018-05-15

4. Frolov, S.M., Dubrovskii, A.V., Ivanov, V.S.: Three-dimensional numerical simulation of the operation of the rotating-detonation chamber. Russian Journal of Physical Chemistry B 6(2), 276–288 (2012), DOI: 10.1134/S1990793112010071

5. Liou, M.S.: A Sequel to AUSM: AUSM+. Journal of Computational Physics 129(2), 364–382 (1996), DOI: 10.1006/jcph.1996.0256

6. Hirsch, C.: Numerical computation of internal and external flows, 2nd Edition. Wiley (1990)

7. Marinov, N.M., Pitz, W.J., Westbrook, C.K., Hori, M., Matsunaga, N.: An experimental and kinetic calculation of the promotion effect of hydrocarbons on the NO-NO2 conversion in a flow reactor. Symposium (International) on Combustion 27(1), 389–396 (1998), DOI: 10.1016/S0082-0784(98)80427-X

8. Kee, R.J., Miller, J.A., Jefferson, T.H.: Chemkin: a general-purpose, problem-independent, transportable Fortran chemical kinetics code package. Sandia National Laboratories Report SAND80-8003 (1980)

9. CHEMKIN. A software package for the analysis of gas-phase chemical and plasma ki-netics. CHE-036-1. Chemkin collection release 3.6. Reaction Design, September 2000

10. Wilcox, D.C.: Turbulence modeling for CFD. DCW Industries, Inc. La Canada (1993)

11. Transport. A software package for the evaluation of gas-phase, multicomponent transport properties. TRA-036-1, CHEMKIN collection, release 2000

12. Connaire, M. O., Curran, H J., Simmie, J. M., Pitz, W. J., Westbrook, C.K.: A comprehensive modeling study of hydrogen oxidation. International Journal of Chemical Kinetics 36(11), 603–622 (2004), DOI: 10.1002/kin.20036

13. Smirnov, N.N., Nikitin, V.F., Alyari-Shourekhdeli, S.: Transitional regimes of wave propagation in metastable systems. Combustion, Explosion, and Shock Waves 44(5), 517–528 (2008), DOI: 10.1007/s10573-008-0080-3

14. Maas, U., Pope, S.: Simplifying chemical kinetics: Intrinsic low-dimensional manifolds in composition space. Combustion and Flame 88(3), 239–264 (1992), DOI: 10.1016/0010-2180(92)90034-M

15. APK-5 documentation. http://compcenter.org/super-evm-apk-5, accessed: 2018-05-15

16. Smirnov, N.N., Penyazkov, O.G., Sevrouk, K.L., et al.: Detonation onset following shock wave focusing. Acta Astronautica 135, 114–130 (2017), DOI: 10.1016/j.actaastro.2016.09.014

17. Betelin, V.B., Kushnirenko, A.G., Smirnov, N.N., et al.: Numerical investigations of hybrid rocket engines. Acta Astronautica 144, 363–370 (2018), DOI: 10.1016/j.actaastro.2018.01.009